Bola-Amphiphilic Dendrimer Enhances Imatinib to Target Metastatic Ovarian Cancer via β-Catenin-HRP2 Signaling Axis

Zeyu Shi, Margarita Artemenko, Weiyu Yu, Ming Zhang, Canhui Yi, Peng Chen, Shuting Lin, Zhancun Bian, Baoping Lian, Fanzhen Meng, et al.

ACS APPLIED MATERIALS & INTERFACES

www.acsami.org
Research Article

Bola-Amphiphilic Dendrimer Enhances Imatinib to Target Metastatic Ovarian Cancer via β-Catenin-HRP2 Signaling Axis

Zeyu Shi,◆ Margarita Artemenko,◆ Weiyu Yu, Ming Zhang, Canhui Yi, Peng Chen, Shuting Lin, Zhancun Bian, Baoping Lian, Fanzhen Meng, Jiaxuan Chen, Tom Roussel, Ying Li, Karen K. L. Chan, Philip P. C. Ip, Hung-Cheng Lai, Sally K. Y. To, Xiaoxuan Liu,* Ling Peng,* and Alice S. T. Wong*

Cite This: https://doi.org/10.1021/acsami.4c12857

ABSTRACT: Ovarian cancer is the leading cause of death among all gynecological malignancies, and drug resistance renders the current chemotherapy agents ineffective for patients with advanced metastatic tumors. We report an effective treatment strategy for targeting metastatic ovarian cancer involving a nanoformulation (Bola/IM)—bola-amphiphilic dendrimer (Bola)-encapsulated imatinib (IM)—to target the critical mediator of ovarian cancer stem cells (CSCs) CD117 (c-Kit). Bola/IM offered significantly more effective targeting of CSCs compared to IM alone, through a novel and tumor-specific β-catenin/HRP2 axis, allowing potent inhibition of cancer cell survival, stemness, and metastasis in metastatic and drug-resistant ovarian cancer cells. Promising results were also obtained in clinically relevant patient-derived ascites and organoids alongside high tumor-oriented accumulation and favorable pharmacokinetic properties in mouse models. Furthermore, Bola/IM displayed synergistic anticancer activity when combined with the first-line chemotherapeutic drug cisplatin in patient-derived xenograft mouse models without any adverse effects. Our findings support the use of Bola/IM as a nanoformulation to empower IM, providing targeted and potent treatment of metastatic ovarian cancer. Our study thus represents a significant advancement toward addressing the unmet medical need for improved therapies targeting this challenging disease.

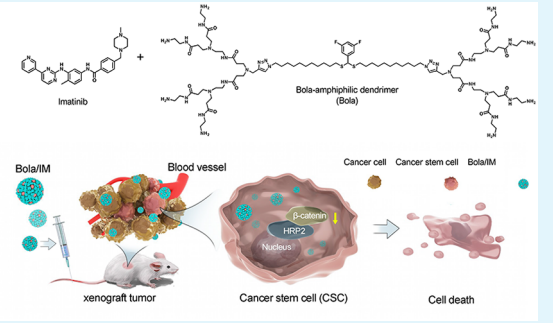

KEYWORDS: *cancer stem cells, targeted therapy, dendrimer, nanovector, chemoresistance, ovarian cancer*

1. INTRODUCTION

Ovarian cancer is the most lethal gynecological malignancy worldwide.[1,2] Being asymptomatic, more than 75% of ovarian cancer cases are diagnosed at an advanced metastatic stage.[3] Platinum/taxane-based chemotherapy is the first-line standard approach used for treating unresectable ovarian cancer[4] but is greatly hindered by intrinsic and acquired chemoresistance. While metastatic tumors are initially sensitive to this chemotherapy, 70% of patients will experience recurrence, which is the major cause of mortality, with a 5-year survival rate of <25%.[5] Thus, there is an urgent need for new therapeutic strategies that can provide increased specificity and efficacy in treating metastatic drug-resistant ovarian cancer.

Cancer stem cells (CSCs) are a small subpopulation of tumor cells that possess a high capacity for self-renewal and multilineage differentiation, tumor initiation, chemoresistance, and metastasis.[6] As such, targeting CSCs represents a critically important strategy in treating metastatic, chemoresistant cancers. We have reported a critical role for receptor tyrosine kinase c-Kit (also known as CD117) in CSCs. Not only does c-Kit serve as a marker of ovarian CSCs, but it also determines their stem phenotype.[7] While activating c-Kit mutations have not been found in ovarian cancer, increased c-Kit expression has been correlated with poorer patient outcomes.[7] Moreover, c-Kit is hyperactivated in tumor-infiltrating immune cells,[8] suggesting that targeting c-Kit may also relieve immunosuppression in the tumor microenvironment.

One ideal candidate for targeting c-Kit is imatinib (IM, Scheme 1a), an FDA-approved anticancer drug shown to inhibit c-Kit, Bcr/Abl, and platelet-derived growth factor receptors.[9] However, clinical trials have shown that IM alone or in combination with docetaxel/paclitaxel has little or no positive effect on overall response or progression-free survival rates in patients with primary or recurrent ovarian cancer (www.clinicaltrials.gov: NCT00510653, NCT00216112, and NCT00840450). Furthermore, while the use of a daily dose of 400 mg IM is generally well-tolerated, there have been rare but nevertheless lethal hematological and hepato/cardiac toxicities

Received: July 31, 2024
Revised: December 12, 2024
Accepted: December 13, 2024

Scheme 1. (a) Chemical Structure of Imatinib (IM) and Bola-Amphiphilic Dendrimer (Bola). (b) Schematic Illustration of Cancer Stem Cell Targeted Recruitment of Bola-Amphiphilic Dendrimer Encapsulated Imatinib (Bola/IM)

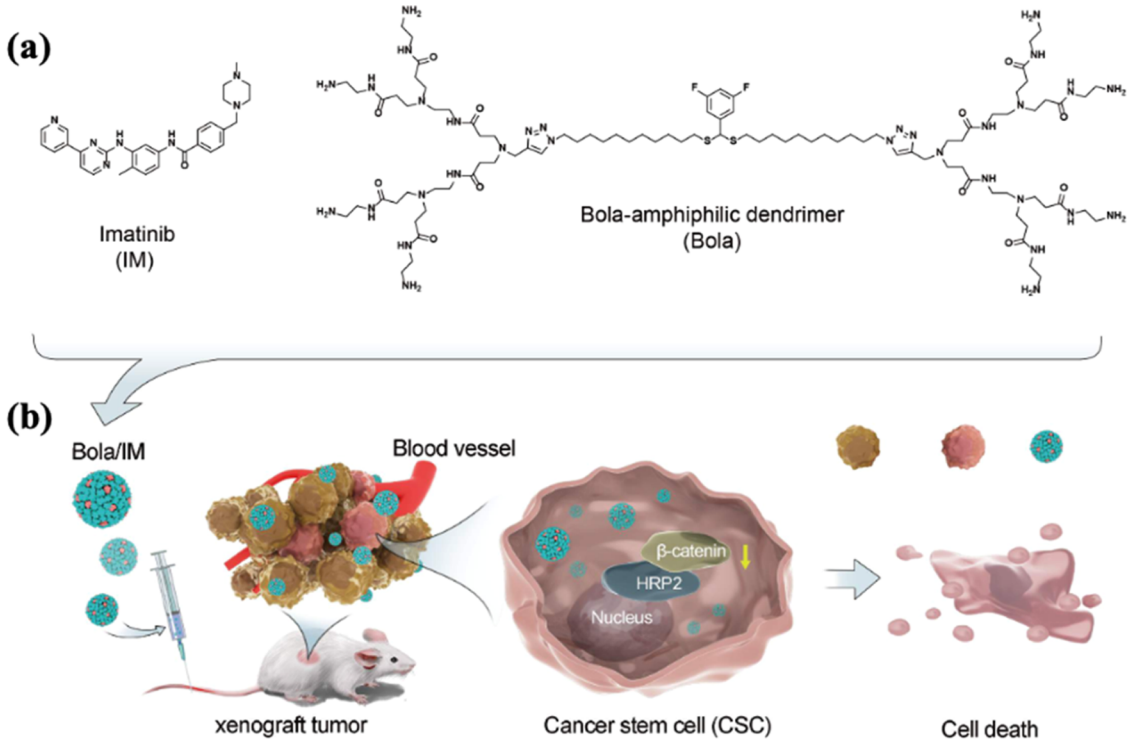

that also need to be considered and addressed.[10] A lower dose regimen that allows safe and effective antitumor efficacy is therefore urgently needed.

In recent years, there has been significant progress in the development of nanotechnology-based drug delivery to enhance the effectiveness of anticancer drugs while minimizing their side effects[11−13] by passively targeting the tumor via the enhanced permeability and retention (EPR) effect.[14−17] This phenomenon is unique to the tumor microenvironment in which a leaky vasculature and dysfunctional lymphatic drainage promote the accumulation and retention of nanosized particles within the tumor lesion, increasing the local concentration of drug molecules and therefore better anticancer activity.

A myriad of nanomaterials such as lipid nanoparticles, polymers, peptides, and proteins have thus been developed to exploit this EPR effect for tumor-targeted drug delivery in cancer treatment.[11,13] Dendrimers, a special class of synthetic polymers with radially symmetric and well-defined structures, have emerged as precision nanomaterials in drug delivery by virtue of their precisely controllable structure and cooperative multivalence.[18,19] In particular, amphiphilic dendrimers have proven to be very useful in the construction of modular self-assembling nanosystems for drug delivery.[20,21] Composed of distinct hydrophobic chains and hydrophilic dendrons, these amphiphilic dendrimers are able to self-assemble into nanoassemblies similar to lipids while retaining their unique dendrimer structural properties.[22−25] We previously developed bola-amphiphilic poly(amidoamine) (PAMAM) dendrimers for nucleic acid delivery, comprising a hydrophobic "bola-lipid" core and two hydrophilic dendron terminals.[26,27] We designed the bola-amphiphilic scaffold to mimic the strong assembly properties of bola-amphiphiles found in extremophile archae bacteria.[28] To enable cancer cell-specific delivery, we incorporated a thioacetal group into our bola-amphiphilic dendrimers thus rendering them responsive to the high level of reactive oxygen species (ROS) in cancer cells.[26,27] Fluorine tags introduced at the core of the dendrimer scaffold also enable the tracking of ROS-responsive delivery using ^{19}F-NMR.[27,29]

In this study, we report for the first time the ability of the bola-amphiphilic dendrimer of generation 2 (referred to hereafter as Bola, Scheme 1a) to encapsulate the anticancer drug IM and form a stable nanoparticulate formulation (Bola/IM) for targeting metastatic ovarian cancer (Scheme 1b). Importantly, low doses of Bola/IM, via a novel β-catenin/HRP2 axis, more effectively targeted ovarian CSCs compared to high-dose IM treatment alone and avoided toxicity in a mouse model of metastatic ovarian cancer. In addition, Bola/IM combined with the chemotherapeutic drug cisplatin demonstrated a synergistic anticancer effect in patient-derived ascite models with no adverse side effects. These results highlight the therapeutic potential of Bola/IM in metastatic ovarian cancer, for which an efficacious treatment is urgently required.

2. MATERIALS AND METHODS

2.1. Experimental Animals. All animal studies conducted were ethically approved by the Committee on the Use of Live Animals in Teaching and Research at The University of Hong Kong, in accordance with the regulations outlined in the Animals (Control of Experiments) Ordinance of Hong Kong.

2.2. Chemicals. IM was obtained from MedChemExpress (Township). Cisplatin and paclitaxel were obtained from Calbiochem (San Diego). Vinblastine was purchased from Sigma (St. Louis). *N*-acetyl-L-cysteine (NAC) was purchased from Calbiochem (Rahway).

2.3. Dendrimer Synthesis. The dendrimer Bola was synthesized according to the well-established protocols in our group.[25,26] Specifically, to a solution of the ester-terminating dendrimer starting material (66.8 mg, 0.036 mmol) in methanol (3.0 mL) was slowly added ethylenediamine (5.1 mL, 76.9 mmol) under an ice bath in the presence of argon. Then, the reaction mixture was stirred for 72 h at 30

https://doi.org/10.1021/acsami.4c12857
ACS Appl. Mater. Interfaces XXXX, XXX, XXX−XXX

°C until the infrared spectrum showed the complete disappearance of the ester functions in the starting material. The reaction solution was evaporated under a vacuum. The resulting residue was purified by precipitation with ether and methanol three times. The product was then dialyzed using a dialysis bag (M_W cutoff 2000) and lyophilized. After the dialysis and lyophilization cycles were repeated three times, the final dendrimer Bola was obtained as a white solid (63 mg, yield: 85%).

2.4. Preparation of Nanoformulation of Imatinib (IM) with the Bola-Amphiphilic Dendrimer (Bola). The Bola-amphiphilic dendrimer (Bola) was used to encapsulate IM via a film dispersion method. Bola and IM were dissolved in a mixed solvent (chloroform/methanol = 3:2, vol/vol) at different mass ratios (w/w 16:2, 16:4, and 16:8) (w/w refer to weight/weight) at 25 °C for 10 min under stirring. Then evaporation was performed to remove the solvent using a vacuum rotary to form a dry film. The resulting dried film was resuspended in ultrapure water and allowed to stand at 4 °C for 4 h. Then filtration was performed through a 0.45-μm polycarbonate membrane (Millipore Co.) to remove the nonencapsulated IM. The nanoformulations were subsequently lyophilized. The amount of IM encapsulated in the micelles was measured using high-performance liquid chromatography (HPLC) analysis (λ = 254 nm). The same procedures were performed to prepare blank Bola micelles without adding IM. The drug-loading efficiency and encapsulation efficiency of the dendrimers were calculated using the following formula

$$\text{loading efficiency} = \frac{\text{experimental IM loading}}{\text{dendrimer} + \text{experimental IM loading}} \times 100\%$$

$$\text{encapsulation efficiency} = \frac{\text{experimental IM loading}}{\text{theoretical IM loading}} \times 100\%$$

2.5. Transmission Electron Microscopy (TEM). The size and morphological characteristics of Bola/IM complexes were examined using transmission electron microscopy. 4.0 mL of solution containing Bola/IM was added onto a Formvar carbon-coated copper grid and air-dried, followed by staining with 2.0% (w/v) uranyl acetate (Sigma-Aldrich, St. Louis) and air-dry before measurement. Isolated nanoparticles were fixed with 4.0% (w/v) neutral buffered formaldehyde and applied onto a Formvar caron-coated copper grid for 20 min. The grids were postfixed with 1.0% (w/v) glutaraldehyde (Sigma-Aldrich, St. Louis) and then stained with 2.0% (w/v) uranyl acetate and allowed to air-dry before measurement. TEM images were performed using a JEOL 2100F analytical electron microscope (Tokyo, Japan) at an accelerating voltage of 200 kV.

2.6. Nanoparticle Tracking Analysis (NTA). Nanoformulations in liquid suspension were loaded into a sample chamber of NanoBrookOmni (Brookhaven) for particle size and ζ-potential analysis.

2.7. Dynamic Light Scattering (DLS). The size distribution and ζ-potential of Bola/IM (100 or 200 μM) were evaluated using dynamic light scattering (DLS) and laser Doppler electrophoresis techniques, respectively, employing a NanoBrookOmni instrument (Brookhaven, State of New York). Each measurement was performed 3 times.

2.8. Cell Lines and Cell Culture. The human ovarian carcinoma cell line HEYA8 was generously provided by Dr J Liu from MD Anderson Cancer Center, Houston, TX, while SKOV3 cells were acquired from ATCC. Primary tumor samples were collected from ovarian cancer patients with their informed consent and approval from the University of Hong Kong Institutional Review Board. The isolation and culture of CSCs from SKOV3 and HEYA8 were conducted as previously described.[7] HEYA8 CSCs were used in peritoneal metastasis mouse experiments, while SKOV3 cells were employed in *in vivo* biodistribution and penetration tests.

2.9. Cell Viability Assay. Cell viability was assessed using colorimetric MTT (3-(4,5-dimethylthiazol-2-yl)-2,5- diphenyltetrazolium bromide) assay following the manufacturer's instructions (Sigma). For tumor spheroids and organoids, samples were first collected and pelleted in tubes, 10% MTT solution was added and incubated for 4 h at 37 °C. Then cell pellets were resuspended in 300 mL DMSO and transferred to a 96-well plate. Analysis was performed at a wavelength of 570 nm by using a microplate reader (Bio-Rad).

2.10. Spheroid Formation Assay. Isolation and culture of HEYA8 and SKOV3 were performed as previously described.[7] Briefly, 5000 cells/mL were seeded in a 100 mm ultralow attachment culture plate with serum-free stem cell-selective medium. After 5−7 days, once spheroids of ∼100 μm were formed, they were harvested and transferred to 100 mm cell culture plates containing the full medium for 2 days. Then, adherent cells were dissociated into a single-cell suspension and reseeded in a 100 mm ultralow attachment culture plate with serum-free stem cell-selective medium for another 5−7 days. On day 7, images of all spheroids were captured, and their sizes and quantities were analyzed using ImageJ Fiji.

2.11. Reverse Transcription and Quantitative-Polymerase Chain Reaction (RT-qPCR). Total RNA was extracted with Trizol reagent (Invitrogen) according to the manufacturer's instructions. cDNA was synthesized using a First Strand cDNA synthesizer kit (Invitrogen). qPCR was conducted using specific primer sequences as follows: Bmi1 Forward: 5′-ATG TGT GTG CTT TGT GGA G-3′, Reverse: 5′-AGT GGT CTG GTC TTG TGA AC-3′; Nanog Forward: 5′-AAG ACA AGG TCC CGG TCA AG-3′, Reverse: 5′-CCT AGT GGT CTG CTG TAT TAC-3′; Oct4 Forward: 5′-ATC CTG GGG GTT CTA TTT GG-3′, Reverse: 5′-TCT CCA GGT TGC CTC CT-3′; CD133 Forward: 5′-AGT CGG AAA CTG GCA GAT AGC-3′, Reverse: 5′-GGT AGT GTT GTA CTG GGC CAA T-3′; CD44 Forward: 5′-CTG CCG CTT TGC AGG TGT A-3′, Reverse: 5′-CAT TGT GGG CAA GGT GCT ATT-3′; ALDH1 Forward: 5′-CTG CTG GCG ACA ATG GAG T-3′, Reverse: 5′-CGC AAT GTT TTG ATG CAG CCT-3′; β-actin Forward: 5′-TCA CCG AGG CCC CTC TGA ACC CTA-3′, Reverse: 5′-GGC AGT AAT CTC CTT CTG CAT CCT-3′. qPCR was carried out using AceQ qPCR SYBR Green Master Mix (High ROX Premixed) Kit (Vazyme) following the manufacturer's instructions. mRNA levels were normalized to the expression of β-actin using $2^{-\Delta\Delta Ct}$ method. Any nonspecific signals from primer dimers were eliminated through nontemplate controls and dissociation curve analysis.

2.12. Western Blotting. Cells were lysed in RIPA lysis buffer containing 50 mM Tris−HCl, 150 mM NaCl, 0.5% sodium deoxycholate, 1.0% NP-40, 0.1 mM PMSF, 0.5 mg/mL leupeptin, 1.0 μM pepstatin, and 0.3 μM aprotinin. Total proteins were separated by 7.5−10% separating SDS-PAGE gel and transferred onto a nitrocellulose membrane. The proteins were blocked with 5% nonfat milk and incubated with primary antibodies overnight at 4 °C: P-glycoprotein (Abcam, ab202976, 1:1000), ABCG2 (CST, 4477, 1:1000), HRP2 (Invitrogen, XC3539332A, 1:1000), β-actin (Sigma, A5316, 1:5000), β-catenin (CST, 2698S, 1:5000), phospho-c-Kit (Biodragon, BD-PP1302, 1,1000), followed by secondary antibody Goat anti-Rabbit IgG (H + L)-HRP conjugate (Bio-Rad, 1706515, 1:3,000), Goat anti-Mouse IgG (H + L)-HRP conjugate (Bio-Rad, 1706516, 1:3000) incubation for 1 h. Protein signals were visualized using Western Lightning Plus Enhanced Chemiluminescence (PerkinElmer), and band intensities were quantified using ImageJ.

2.13. Drug Efflux Test. Drug efflux test was performed using Multidrug Resistance Direct Dye Efflux Assay kit (Merck), according to manufacturer's instruction. Briefly, cells were collected and disaggregated with 2 mM EDTA/PBS in a single-cell suspension with cold efflux buffer. Then, cells were incubated with $DiOC_2(3)$ solution on ice for 30 min. After that, cells were washed and distributed into 3 different tubes, containing vinblastine solution, DMSO, and cold efflux buffer. Tubes with DMSO and vinblastine were incubated at 37 °C for 4 h and cold efflux buffer on ice, all protected from light. Cells were then washed to stop the efflux reaction, stained with PI solution, and resuspended in PBS. Flow cytometry on BD FACSAria III (BD Biosciences) was performed at excitation of 488 nm. FlowJo software was used for the data analysis. Only live cells were included, and FITC signal was used as an indicator of $DiOC_2(3)$ efflux intensity.

2.14. Subcellular Fractionation. Cells were lysed in 500 μL of CLB buffer (10 mM HEPES, 1.0 mM KH_2PO_4, 10 mM NaCl, 5.0 mM $NaHCO_3$, 5.0 mM EDTA, 0.50 mM $MgCl_2$, 1.0 mM $CaCl_2$,) and

https://doi.org/10.1021/acsami.4c12857
ACS Appl. Mater. Interfaces XXXX, XXX, XXX−XXX

subjected to mechanical disruption using a glass homogenizer following the addition of sucrose; crude nuclear extracts were obtained through centrifugation at 6300*g* for 5 min at 4 °C. These extracts were then washed with TSE buffer (10 mM Tris, 300 mM sucrose, 1.0 mM EDTA, 0.10% IGEPAL-CA 630 v/v, pH 7.5) to remove debris and store it for future use.

2.15. Immunoprecipitation-Mass Spectrometry. The nuclear extracts were prepared as described above. 500 mg nuclear extract diluted in 500 mL IP lysis buffer was precleared by incubating with 20 mL protein A/G agarose beads for 2 h at 4 °C. Then the precleared nuclear proteins were mixed with 25 mL b-catenin primary antibody with Sepharose bead conjugated or 25 mL rabbit IgG control with Sepharose bead conjugated at 4 °C overnight. The beads were washed by IP lysis buffer 3 times and preurea wash buffer (20 mM Tris pH 7.5, 150 mM NaCl). 50 mL of urea elution buffer (8 M Urea, 25 mM ammonium bicarbonate) was added and incubated at 65 °C for 15 min. The beads were pelleted by centrifugation, and the supernatant was transferred to a new 1.5 mL tube, followed by further trypsin digestion and peptide purification for mass spectrometry (MS) analysis.

2.16. Immunoprecipitation. The nuclear extracts were prepared as described above. 300 mg nuclear extract diluted in 500 mL IP lysis buffer was precleared by incubating with 20 mL protein A/G agarose beads (Santa Cruz) for 2 h at 4 °C. Then the precleared nuclear proteins were mixed with primary antibodies overnight. 30 mL prewashed protein A/G agarose plus-agarose beads were added to precipitate the antigen−antibody complexes at 4 °C for 1 h. The beads were then washed with IP lysis buffer 3 times and diluted with 30 μL of 2× loading buffer. Samples were denatured at 95 °C for 5 min, followed by brief centrifugation to pellet the beads. Eluted protein was then analyzed by Western blot.

2.17. Immunofluorescence Microscopy. Cells seeded in each well of a 24-well plate on coverslips were fixed with 4.0% paraformaldehyde. Permeabilization was done with 0.10% Triton for 5 min and followed by 15 min blocking with 5.0% bovine serum albumin. Cells were incubated with primary HRP2 antibody (Invitrogen, 1:50) for 1 h, washed with PBS 3 times, and then incubated with secondary Cy3 antibody (ThermoFisher, 1:200) for 1 h. For patient-derived samples, tissues were fixed with 4.0% paraformaldehyde for 20 min and followed by blocking with 5.0% bovine serum albumin. Tissues were treated with 0.50% Triton-X100 to permeabilize before being exposed to primary antibody (1:50) overnight at 4 °C. Following PBS washes, the tissues were then incubated with secondary antibody mixture (1:200) for 2 h at room temperature and mounted with DAPI. Signals were visualized using a Carl Zeiss LSM 980.

2.18. Small Interfering RNA Transfection. Nonspecific (GGC TAC GTC CAG GAG CGC A) and HRP2 siRNAs (CCA AGA AAU CAG CGA AGA A) were purchased from Invitrogen. Cells were transfected with 20 nM siRNA using Lipofectamine 2000 following the manufacturer's instructions (ThermoFisher).

2.19. *In Vivo* Tumor Peritoneal Metastasis Assay. All experiments involving mice were conducted following the guidelines approved by Committee on the Use of Live Animals in Teaching and Research at the University of Hong Kong, in accordance with the Animals (Control of Experiments) Ordinance of Hong Kong. 2.0×10^6 cells were intraperitoneally (ip) injected into 6−8 week old female NOD/SCID mice. Body weights were measured every other day. For IM dosage valuation, mice were injected with PBS, IM 2.5 mg/kg or 5.0 mg/kg every 2 days for 2 weeks after 1 week of tumor cell injection. Mice were then sacrificed, and mesentery metastasis nodules were counted. For Bola/IM estimation, after 1 week following tumor cell injection, mice were randomly divided to receive PBS, empty Bola (1.0 mg/kg), Bola/IM (1.0 mg/kg), and naked IM (2.5 mg/kg). PBS, empty Bola, and naked IM were treated every 2 days, and Bola/IM was received on Day 7, 11, 15, and 19. PBS, empty Bola, and naked IM were used as controls. For CDDP combination therapy, after 1 week following tumor cell injection, mice were randomly divided to receive PBS, naked IM (2.5 mg/kg), Bola/IM (1.0 mg/kg), and Bola/IM (1.0 mg/kg) + CDDP (5.0 mg/kg). PBS and naked IM were treated every 2 days, Bola/IM and CDDP combination were received on Day 7, 11, 15, and 19. PBS, empty Bola and naked IM were used as controls. At the end of experiments, mice were sacrificed and peritoneal metastases were counted. Tumor and organs (heart, lungs, liver, kidneys, spleen, brain, blood) were collected, fixed in formalin and embedded in paraffin for H&E and immunohistochemical staining. Blood plasma was collected for biochemical marker analysis using Infinity AST(GOT) kit, Infinity ALT(GPT) kit (ThermoFisher), Creatinine LiquiColor Test kit, CK-MB Liqui-UV Test kit, Direct Bilirubin LiquiColor Test kit (Stanbio) and Urea Assay kit (Abcam). Whole blood or peritoneal fluid was stained in Wright stain.

2.20. *In Vivo* Biodistribution Study and Tumor Penetration. All protocols were endorsed by the Institutional Animal Care and Use Committee of China Pharmaceutical University and executed in accordance with the established guidelines and policies. The approval number is "2023−09−009". Female BALB/c nude mice (6 weeks old) were from Beijing Vital River Laboratory Animal Technology Co., Ltd. (Beijing, China). The mice were maintained in the China Pharmaceutical University Laboratory Animal Center during the experiment, and all mice were housed in specific pathogen-free conditions according to the current Chinese regulation of China Pharmaceutical University. 5.0×10^6 SKOV3 cells were inoculated subcutaneously to the mice. After 3 weeks, the mice bearing SKOV3 xenograft tumors were randomly divided into 3 groups (n = 3/group) and then administrated with PBS (phosphate buffer saline), free DiR (40 μg/kg), and Bola/IM/DiR (4.0 mg/kg of Bola, 1.0 mg/kg of IM, 40 μg/kg of DiR) *via* tail vein of mice, respectively. The *in vivo* fluorescence images were recorded at 0.5, 2, 8, 12, 24, and 48 h after intravenous administration of Bola/IM/DiR. And the mice were anaesthetized using isoflurane gas and then visualized by using the small animal live optical imaging system (PerkinElmer, IVIS@ spectrum) (excitation wavelength 740 nm and emission wavelength at 770 nm). Then, mice were sacrificed after 48 h, and the excised major organs and tumors were collected for imaging. In the last, the tumor tissue was used to make frozen sections and immunohistochemical tests, blood vessels were labeled with FITC-labeled CD31 and nuclei with DAPI, and sections were then photographed using a laser scanning confocal microscope (ZEISS, LSM880, Germany) to detect the penetration of DiR-labeled Bola/IM in tumor lesion.

2.21. Drug Penetration in Tumor Spheroids. The penetration ability of DiR-labeled Bola/IM in multicellular tumor spheroids was studied using Carl Zeiss LSM 980 (Oberkochen, Germany). Cells were seeded in a low-attachment culture dish containing serum-free medium, allowing 14 days to form tumor spheres. 1.0 mg/mL Bola/IM/DiR were added into culture medium for 5 h, washed with PBS, and fixed with 4.0% formaldehyde at 4 °C for 20 min. Spheroids were then resuspended in 60% glycerol after washing with PBS twice for z-stack imaging. The images were captured from the lower position top up to the center of spheroids every 5 mm at 10× magnification.

2.22. Reactive Oxygen Species (ROS) Assay. Bola/IM/DiR incubated CSCs were treated with NAC for 24 h, and spheroids were collected and resuspended with 100 mL of 1× ROS Assay Stain (Invitrogen) for 60 min. Then spheroids were trypsinized to single cells for flow cytometry analysis (Agilent NovoCyte Quanteon).

2.23. ALDEFLUOR Assay. The ALDEFLUOR assay was conducted according to the manufacturer's instructions (STEMCELL Technologies). Briefly, cells were prepared at 2.0×10^5 cells/mL in activated ALEFLUOR reagent. After centrifugation at 250 g for 5.0 min, the cell pellets were resuspended in ALDEFLUOR Assay Buffer for flow cytometry analysis (Agilent NovoCyte Quanteon).

2.24. Pharmacokinetics Analysis. The bioanalysis condition was specified as follows: LC system (Shimadzu LC-40D system), MS system (Sciex QTRAP 6500+), column (Agilent Eclipse Plus C18, 18 mm, 2.1 × 50 mm^2), column temperature 40 °C, flow rate 0.2 mL/min, electrospray ionization (positive). The mobile phase consisted of 0.1% formic acid in ultrapure water (mobile phase A) and 0.1% formic acid in acetonitrile (mobile phase B). The following gradient profile was used: (1) 1.0 min, 5% B; (2) 2.5 min, 70% B; (3) 6.5 min, 70% B; (4) 7.5 min, 5% B; and (5) 8.0 min, 5% B. IM was extracted from the serum by methanol. The samples were vortexed and centrifuged, and the supernatant was then injected into liquid chromatography with tandem mass spectrometry (LC-MS/MS). The calibration curves and quality

https://doi.org/10.1021/acsami.4c12857
ACS Appl. Mater. Interfaces XXXX, XXX, XXX−XXX

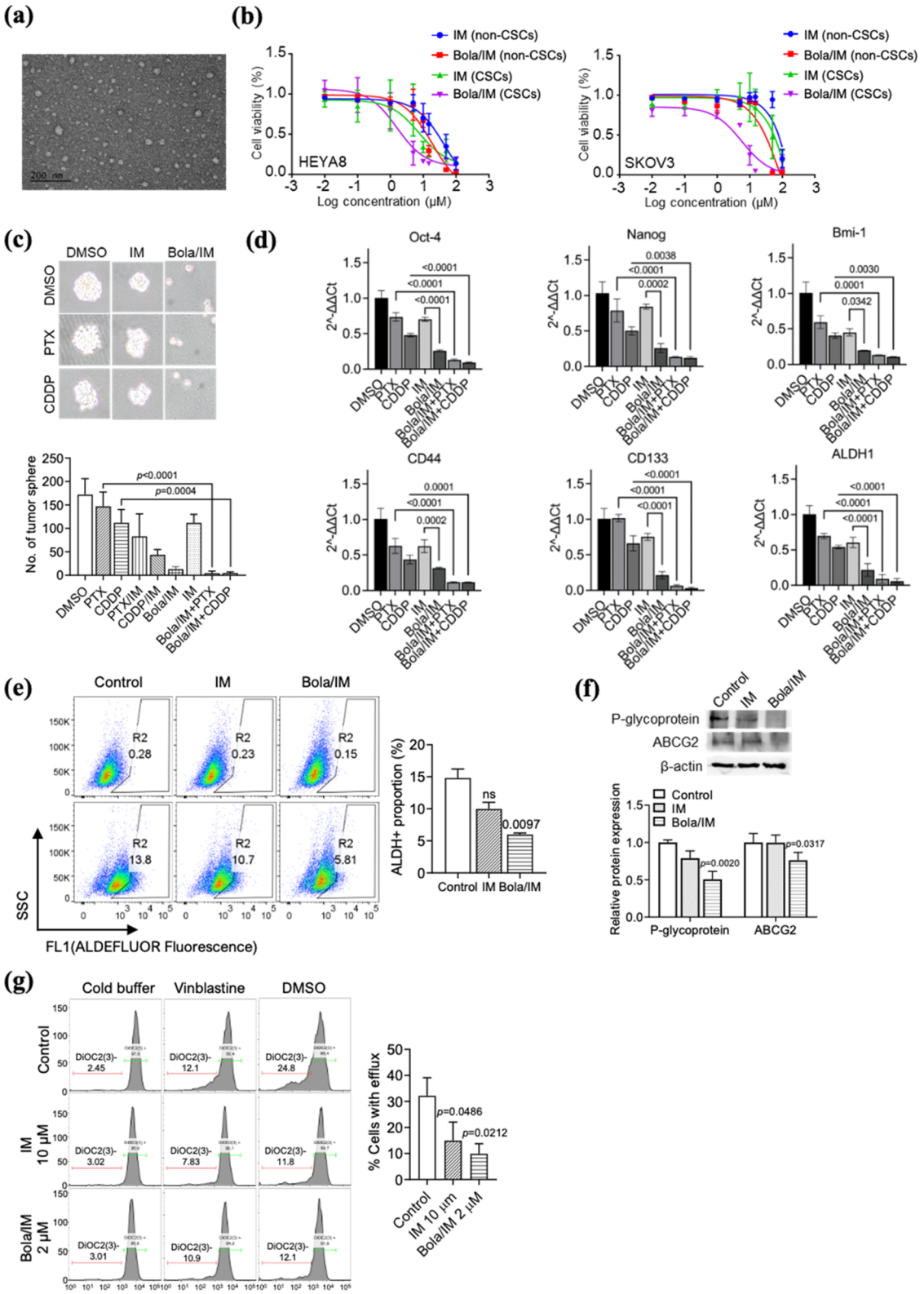

Figure 1. Bola/IM nanoformulation inhibits CSCs *in vitro*. (a) TEM images of Bola/IM. (b) *In vitro* cytotoxicity IC_{50} (μM) values of IM, Bola, and Bola/IM toward non-CSCs and CSCs. (c) Spheroids treated with paclitaxel (PTX) or cisplatin (CDDP) with/without IM or Bola/IM. Pictures were taken at Day 7. Number of tumor spheres were counted, and (d) changes of sternness markers were identified by qRT-PCR in HEYA8 CSCs. β-actin was used as a control, and (e) CSCs were treated with IM or Bola/IM and ALDH activity was measured, (f) cells treated with IM or Bola/IM and expression of P-glycoprotein and ABCG2 were detected by Western blot. β-actin was used as a control, and (g) Bola/IM nanoformulation reduced drug efflux in HEYA8 CSCs. Experiments were repeated 3 times, and data are shown as mean + SD *, $P < 0.05$ *vs* control and ***, $P < 0.001$ *vs* control.

control samples were prepared in blank mouse serum and treated following the same procedure as the samples.

2.25. Immunohistochemistry Staining. Slides with tissue sections were rehydrated. Endogenous peroxidase activity was inhibited

https://doi.org/10.1021/acsami.4c12857
ACS Appl. Mater. Interfaces XXXX, XXX, XXX−XXX

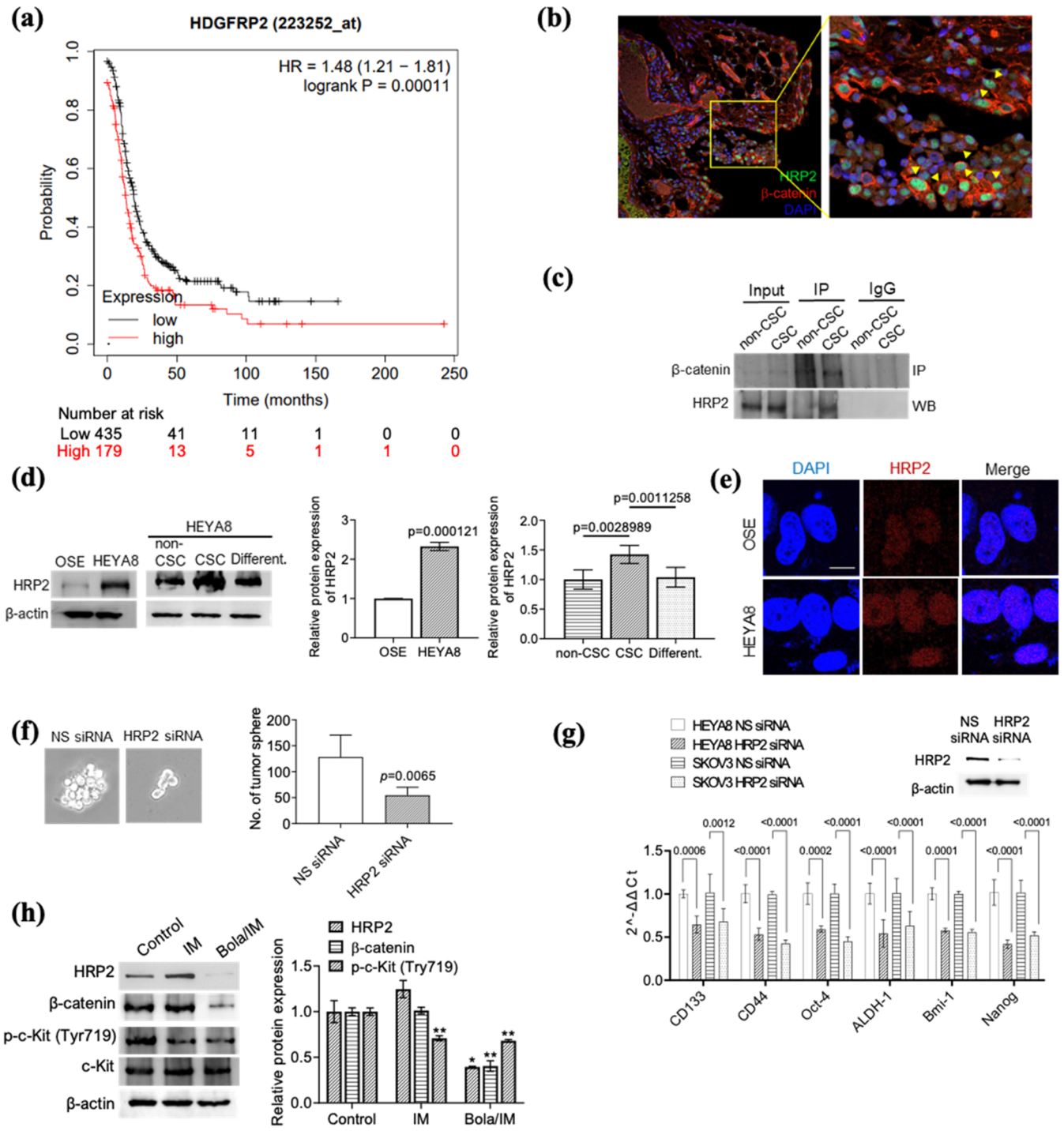

Figure 2. Bola/IM inhibits the β-catenin/HRP2 signaling pathway. (a) Kaplan−Meier analysis of progression-free survival with high or low HRP2 expression for ovarian cancer patients ($P = 0.00011$, log-rank test), (b) nuclear localization of HRP2 and β-catenin in the patient sample were visualized by immunofluorescence on cryosection (yellow arrows), (c) HRP2/β-catenin complexes were detected by Western blot using anti-HRP2 antibody after immunoprecipitation by β-catenin primary antibody with nuclear extracts, (d) western blot analysis of HRP2 expression in OSE, HEYA8, and HEYA8 CSCs, and differentiated cells from spheroids, β-actin was used as a control, (e) expression and distribution of HRP2 in OSE and HEY A8 through immunofluorescence analysis, (f) spheroids were treated with 20 nM HRP2 siRNA or control siRNA and the representative images of tumor spheroids were recorded, (g) changes in sternness markers were identified by RT-PCR. β-actin was used as a control; (h) western blot analysis of HRP2 expression upon IM or Bola/IM treatment at 5 μM. β-actin was used as a control. Experiments were repeated 3 times, and data are shown as mean + SD *, $P < 0.05$ *vs* control. **, $P < 0.01$ *vs* control. ***, $P < 0.001$ *vs* control.

by incubation in 3% hydrogen peroxide. Antigen retrieval was performed with heating slides at 90 °C in a citrate buffer (pH 6.0) and then cooling slides at room temperature. Slides were then incubated with primary antibody solution in a blocking buffer overnight at 4 °C, washed with TBS-T, and incubated with the biotin-conjugated secondary antibody. Slides were then incubated with streptavidin and with DAB solution and counterstained in hematoxylin (Biocare medical). The slides were washed, dehydrated, air-dried, and mounted with coverslips. The DAB positive signal was quantified by using ImageJ Fiji.

https://doi.org/10.1021/acsami.4c12857
ACS Appl. Mater. Interfaces XXXX, XXX, XXX−XXX

2.26. Statistical Analysis. Each experiment was repeated at least 3 times. The normality of the sample distribution was checked with the Shapiro-Wilk test. *t*-test was used for parametric samples, and the Wilcoxon test was used for nonparametric samples with 2 groups. One-way ANOVA was used for multiple comparisons. Two-way ANOVA was used for multiple groups comparison with 2 or more categorial variables. $p < 0.05$ was considered as statistically significant.

3. RESULTS

3.1. Robust Nanoformulation of IM with the Bola-Amphiphilic Dendrimer (Bola). We have successfully exploited amphiphilic dendrimers for the encapsulation of structurally diverse anticancer drugs including doxorubicin, paclitaxel, and rapamycin previously.[23−25,30] These dendrimers self-assemble into supramolecular dendrimer nanomicelles with spacious interior cavities for excellent drug-loading and encapsulation efficiencies. The dendrimers used in these earlier studies were classical amphiphiles composed of a hydrophobic chain component and a hydrophilic PAMAM dendron part. In the present study, we employed bola-amphiphilic dendrimers of generation 2 (Bola)[26,27] for drug encapsulation. Unlike the classical amphiphile dendrimers, Bola features a unique structure comprising a bola-lipid thioacetal core and two PAMAM dendrons at each of two terminals. This distinctive composition holds the potential to form stable formulations for drug encapsulation while allowing for ROS-responsive drug release, offering exciting possibilities for further exploration.

We first studied the drug-loading capacity and encapsulation efficiency of IM by Bola using various ratios of IM and Bola (w/w) (16/2, 16/4, and 16/8). Specifically, the thin film dispersion method was used to encapsulate IM by Bola.[23] These results listed in Table S1a highlight that Bola effectively encapsulates IM with high loading and encapsulation capacities. A maximum drug-loading efficiency of 33% and quantitative drug encapsulation efficiency were obtained for IM-loaded dendrimer nanoformulation (referred to hereafter as Bola/IM) at a mass ratio of 16/8 (w/w) (Figure S1a). We performed all of our further studies at the optimal ratio of Bola/IM (16/4, w/w) considering the stability of nanoformulation.

The IM-loaded dendrimer assemblies (Bola/IM) obtained in this study exhibited a small size and spherical shape, as revealed using transmission electron microscopy (TEM) (Figure 1a). Dynamic light scattering (DLS) analysis further confirmed the small size of the Bola/IM, with an average diameter of approximately 30 nm (PDI: ∼0.2) (Figure S1b) and a ζ-potential of +33 (±3) mV (Figure S1c). These findings collectively demonstrate the successful nanoformulation of Bola/IM, emphasizing its effectiveness in producing small, stable, and well-defined nanoparticles.

3.2. Bola/IM Nanoformulation Inhibits CSC *In Vitro*. With the stable and robust Bola/IM nanoformulation in hand, we first conducted MTT assays to evaluate its therapeutic potential in targeting both CSCs and non-CSCs *in vitro*. Strikingly, the results demonstrated that compared to non-CSCs, CSCs exhibited up to 16-fold higher sensitivity to Bola/IM (Figures 1b and S1d). The IC_{50} values for HEYA8 CSCs and SKOV3 CSCs were determined to be 1.6 and 5.7 μM, respectively; in contrast to 19 μM for HEYA8 non-CSCs and 96 μM for SKOV3 non-CSCs, and 39 μM for normal ovarian surface epithelial (OSE) cells. The significant difference in effective doses between OSE and CSCs suggests that Bola/IM exhibits favorable tolerance in eliminating CSCs. Compared to IM, Bola/IM demonstrated superior efficacy for both CSCs and non-CSCs, yet with remarkably higher potency to target CSCs over non-CSCs (Figures 1b and S1d).

To further investigate the therapeutic efficacy of Bola/IM in treating CSCs, we employed sphere formation assays, which are functional hallmarks of CSC renewal. The results indicated that Bola/IM was significantly more effective in blocking CSC self-renewal compared to naked IM at the same dose (Figure 1c). Moreover, Bola/IM sensitized chemoresistant CSCs to paclitaxel (PTX) and cisplatin (CDDP) (Figure 1c). Notably, treatment with Bola/IM led to marked decreases in CSC stemness markers such as Bmi1, Nanog, Oct4, CD44, CD133, and ALDH1 in comparison to treatment with IM, PTX, or CDDP alone, which was reversed by Bola/IM treatment (Figure 1d). In addition, ALDEFUOR activity was inhibited upon Bola/IM treatment (Figure 1e). In contrast, naked Bola had no effect on cell viability or CSC renewal ability (Figure S2a−c).

Given the potential association between CSC-driven chemoresistance and overexpression of drug efflux pumps on the cell membrane,[31−33] we investigated the impact of Bola/IM on the two major efflux pumps in ovarian CSCs, ABCG2 and P-glycoprotein. Remarkably, treatment with Bola/IM resulted in a considerable decrease in the levels of ABCG2 and P-glycoprotein, whereas equivalent concentrations of IM exhibited no such effect (Figure 1f) and neither naked Bola demonstrated any reduction in P-glycoprotein and ABCG2 expression, as well as drug efflux (Figure S2d,e). These findings demonstrate that Bola/IM effectively inhibits drug efflux, which could explain its ability to overcome chemoresistance (Figure 1g). As cancer cells often have activated macropinocytosis,[34,35] the Bola/IM nanoparticles are able to promote cellular uptake of drug *via* endocytosis, hence bypassing efflux mechanisms. These findings demonstrate the ability of Bola/IM to interfere with CSC self-renewal and overcome chemoresistance by inhibiting drug efflux pumps, altogether highlighting Bola/IM as a promising effective therapeutic strategy for targeting CSCs.

3.3. Bola/IM Inhibits the β-catenin/HRP2 Signaling Pathway. We previously reported that c-Kit could activate β-catenin signaling in mediating chemoresistance in CSCs.[7] Given the effectiveness of Bola/IM in treating CSCs but not non-CSCs while overcoming drug resistance, we sought to investigate whether Bola/IM was involved in the c-Kit-activated β-catenin signaling pathway. To compare the differential interacting partners of β-catenin downstream of c-Kit between non-CSCs and CSCs, we performed coimmunoprecipitation (co-IP) followed by LC-MS/MS proteome analysis (Supporting Information).

Among the potential partners identified, hepatoma-derived growth factor related protein 2 (HRP2) was found to be among the most significantly enriched nuclear proteins in CSCs compared to non-CSCs (9.84-fold) (Figure S3a). Also importantly, a high expression of HRP2 tended to correlate with poor clinical outcomes in ovarian cancer patients (Figure 2a). We also observed a positive association between HRP2 and β-catenin in clinical samples (Figure 2b). The interaction between β-catenin and HRP2 was confirmed by co-IP and Western blot analysis (Figure 2c). The differential levels of β-catenin-HRP2 interaction between CSCs and non-CSCs may be attributed to the higher basal expression of HRP2 in CSCs (Figure 2d). HRP2 expression was lost upon CSC differentiation and was significantly lower in the normal ovarian surface epithelium (OSE) (Figure 2d). Immunofluorescence microscopy further confirmed the nuclear localization of HRP2 (Figure 2e).

https://doi.org/10.1021/acsami.4c12857
ACS Appl. Mater. Interfaces XXXX, XXX, XXX−XXX

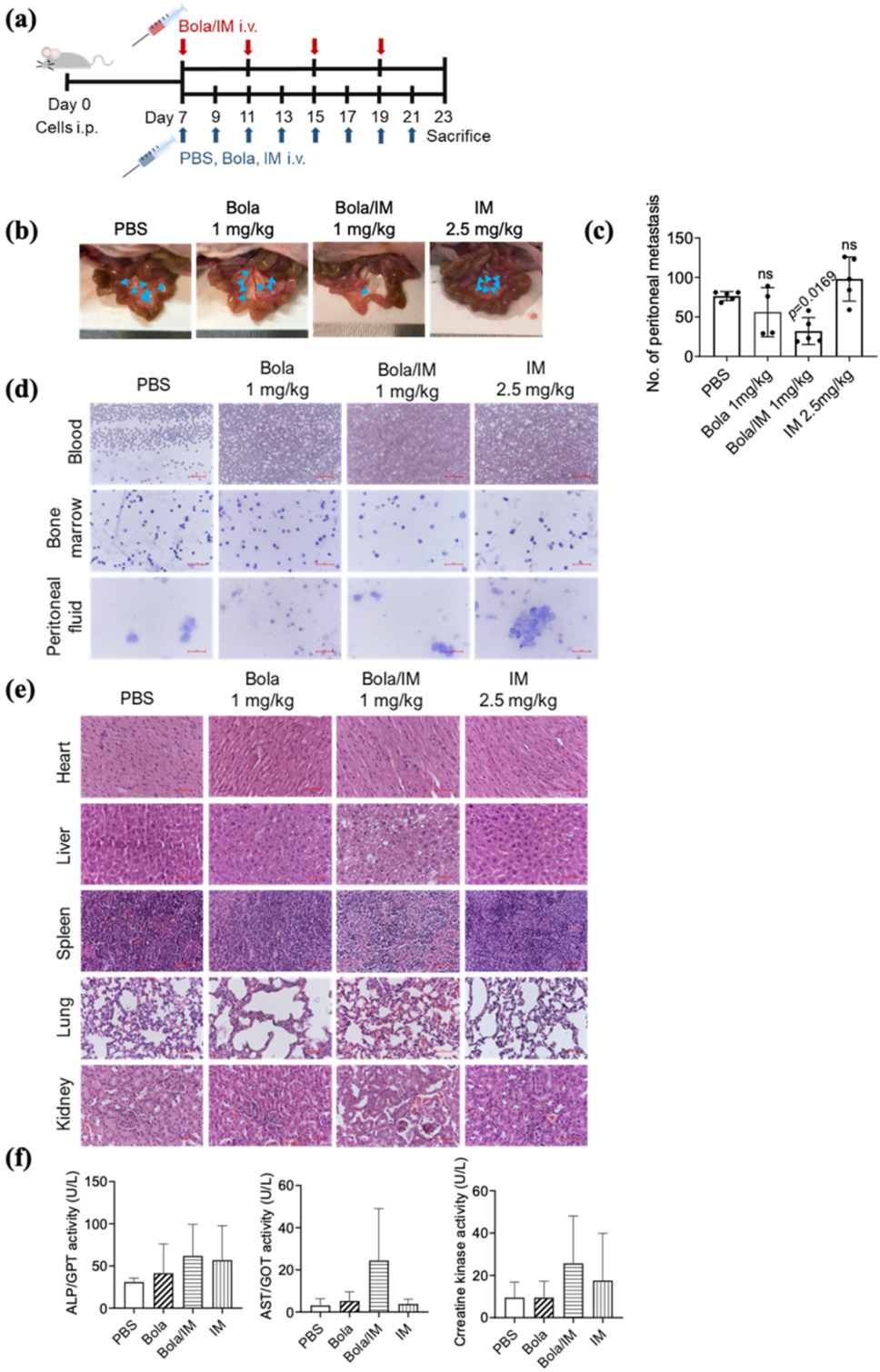

Figure 3. Therapeutic and chemosensitization effects of Bola/IM nanoformulation *in vivo*. (a) Timeline of treatments in tumor-bearing mice (n = 5). (b) Bola/IM nanoformulation inhibits peritoneal metastasis of HEYA8 CSCs at a dose of 1 mg/kg. Mesentery metastasis comparison. Arrows indicate large tumor nodes and (c) peritoneal metastasis number comparison after treatment, (d) Wright stained smears of blood, bone marrow, and peritoneal fluid, (e) morphological characteristics of H&E stained organs and tissues following different treatments including Bola/IM nanoformulation. (f) blood plasma biochemical markers evaluation. Experiments were repeated 3 times, and data are shown as mean + SD. Experiments were repeated 3 times, and data are shown as mean ± SD **, $P < 0.01$ *vs* control. ***, $P < 0.001$ *vs* control

In addition, HRP2 siRNA reduced CSC sphere formation (Figure 2f), and the expression of stemness markers (Bmi1, Oct4, Nanog, CD44, CD133, and ALDH) was reduced (Figure 2g). Western blot showed the knockdown efficiency of HRP2 siRNA (Figure 2g). Notably, treatment with Bola/IM at 5.0 μM significantly inhibited HRP2 and β-catenin expression (Figure 2h), whereas a similar decrease in HRP2 and β-catenin expression was observed only with naked IM at very high

https://doi.org/10.1021/acsami.4c12857
ACS Appl. Mater. Interfaces XXXX, XXX, XXX−XXX

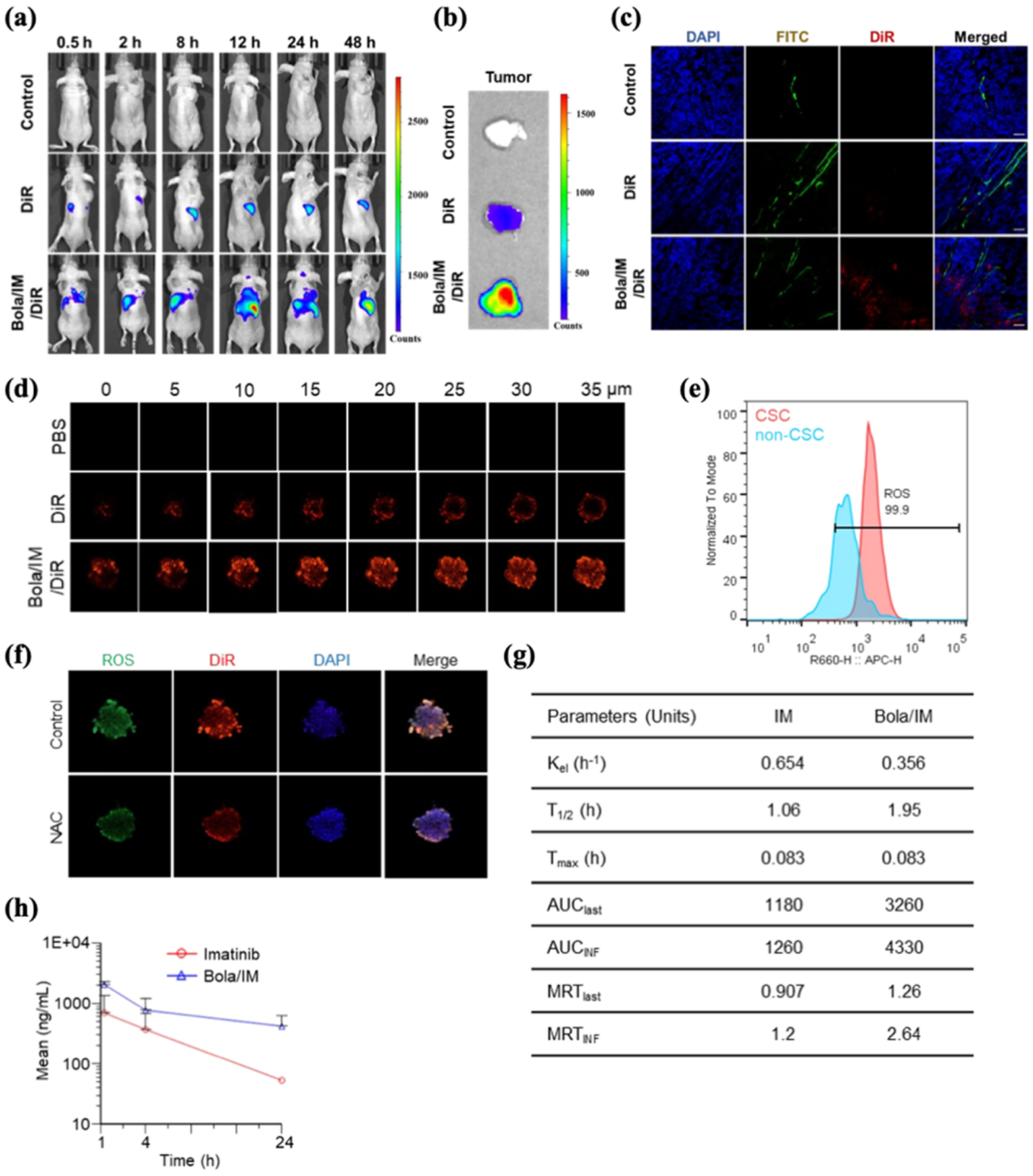

Parameters (Units)	IM	Bola/IM
K_{el} (h^{-1})	0.654	0.356
$T_{1/2}$ (h)	1.06	1.95
T_{max} (h)	0.083	0.083
AUC_{last}	1180	3260
AUC_{INF}	1260	4330
MRT_{last}	0.907	1.26
MRT_{INF}	1.2	2.64

Figure 4. Bola/IM achieves a high tumor-oriented accumulation with enhanced drug delivery efficiency. (a) Nanoparticles incorporated with fluorescent dye were intravenously injected into mice with subcutaneous tumors and imaged at different time points (0.5 h, 2 h, 4 h, 8 h, 12 h, 24 h, and 48 h). (b) Tumors were then harvested at 48 h after i.v. injection, the fluorescent signals of tumors were imaged and (c) significantly improved accumulation and penetration within the tumor lesion. Red signal, DiR; green signal, FITC-tagged CD31 (staining tumor vessels) to show the excellent accumulation penetration of Bola/IM deep within the tumor lesion (scale bar: 50 μm). (d) Penetration of Bola/IM/DiR within tumor spheroids and (e) APC-H histograms showing the ROS levels of CSC and non-CSC. (f) NAC inhibits ROS recruited Bola/IM/DiR accumulation in tumor spheroids. (g) Pharmacokinetic parameters of IM and of Bola/IM in mice following intravenous administration. (h) Plasma concentration−time profile of IM after administration of IM and Bola/IM to mice, respectively. Experiments were repeated 3 times, and data are shown as mean ± SD.

concentration (80 μM) (Figure S3b). Phospho (active)-c-Kit was significantly inhibited by Bola/IM treatment, whereas total c-Kit was unaffected (Figure 2h). These findings are consistent with our previous observations regarding the effect of c-Kit on CSC growth inhibition and provide further evidence of the significantly more pronounced effect of Bola/IM on CSCs compared to that of naked IM. The data also highlight the potential of Bola/IM in targeting the c-Kit/β-catenin-HRP2 signaling pathway in CSCs, which could contribute to its superior therapeutic efficacy.

3.4. Therapeutic Effects of Bola/IM Nanoformulation *In Vivo*.

To evaluate the anticancer activity of Bola/IM *in vivo*, we used a mouse model of metastatic ovarian cancer induced by CSCs (Figure 3a). HEYA8 CSCs were injected intraperitoneally into mice to generate the metastatic ovarian cancer model,[7] then Bola/IM or PBS or IM alone as a control, were administrated intravenously. Remarkably, even at a low dose of 1.0 mg/kg, Bola/IM significantly reduced peritoneal metastases (Figure 3b), while IM alone only showed inhibition at the 5-fold higher dose of 5.0 mg/kg but not at the 2.5-fold higher dose of 2.5 mg/

https://doi.org/10.1021/acsami.4c12857
ACS Appl. Mater. Interfaces XXXX, XXX, XXX−XXX

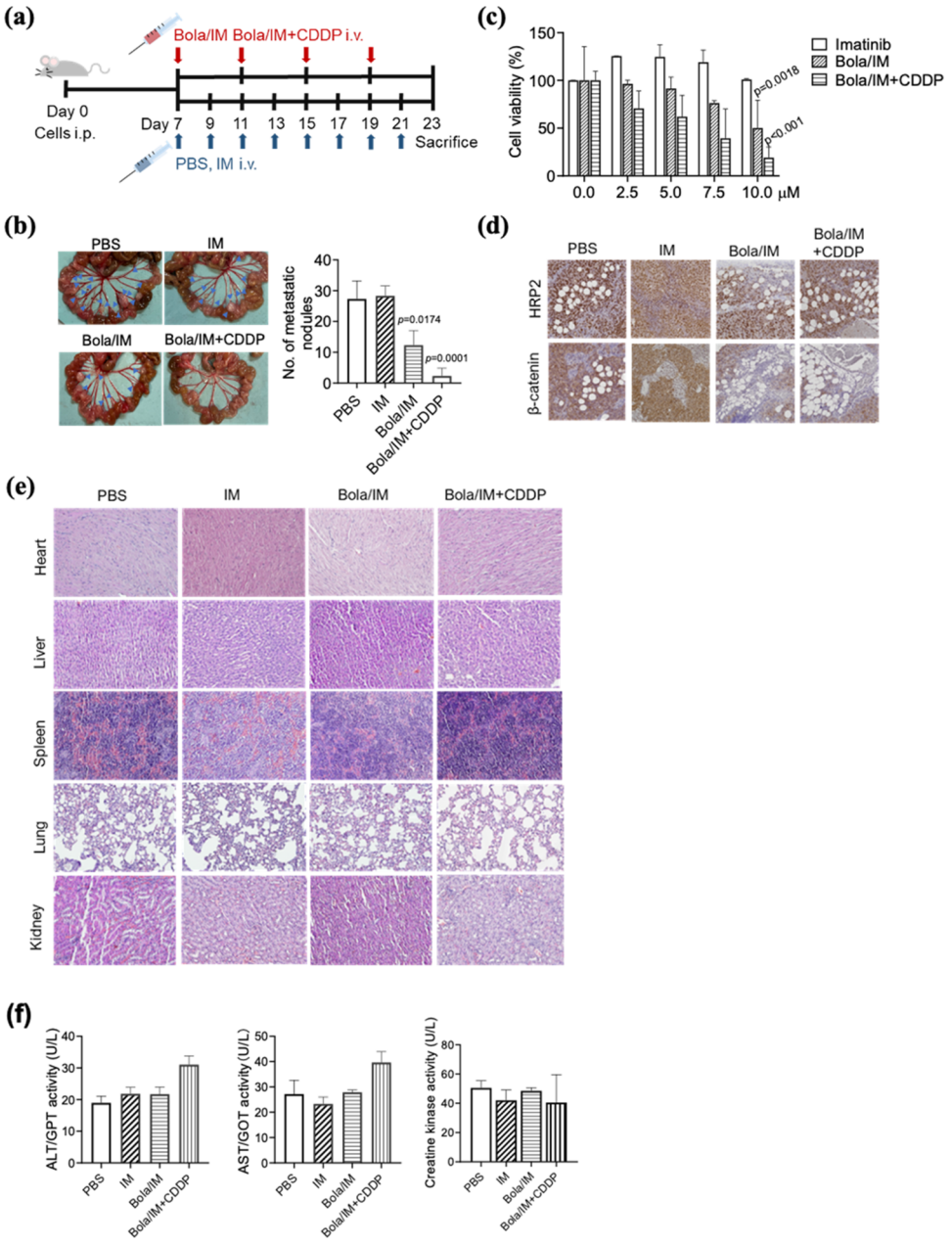

Figure 5. Bola/IM alone and in combination with CDDP decreases malignancy in patient-derived models without severe adverse effects. (a) Timeline of treatments in tumor-bearing mice (n = 5). (b) Cell viability of patient-derived organoids, (c) Mesentery comparison with arrows indicating large tumor nodes; the bar chart showing the number of peritoneal metastatic nodules according to treatment, (d) HRP2 and β-catenin expression levels were detected by immunohistochemistry in the tumor tissues, and (e) Morphological characteristics of organs and tissues of mice treated with Bola/IM alone and in combination with CDDP. H&E stained organs and tissue comparison, (f) Blood plasma biochemical markers evaluation were measured and compared to control injected mice. Experiments were repeated 3 times, and data are shown as mean ± SD *, $P < 0.05$ *vs* control.**, $P < 0.01$ *vs* control. ***, $P < 0.001$ *vs* control.

kg (Figures 3b and S4a), suggesting increased effectiveness of Bola/IM compared to IM alone. Furthermore, the number of tumor nodules was significantly reduced after treatment with Bola/IM (Figure 3c). Importantly, Bola/IM was well tolerated by the mice, as we observed no abnormal behavior or weight loss during the entire treatment period (Figures S4b and S5). In addition, we found no pathological alterations in blood, bone marrow, or peritoneal fluid (Figure 3d). Also, histopathological analysis of the heart, kidney, liver, lung, and spleen showed no considerable alterations such as inflammation, necrotic sites, ischemia, or hyperemia in the treated mice compared to the controls (Figure 3e). Blood chemistry further demonstrated no significant changes in alkaline phosphatase (ALP), aspartate aminotransferase (AST), or creatine kinase activity (Figure 3f), thus confirming the lack of adverse effects of Bola/IM on normal tissue. These findings suggest that Bola/IM has potent and selective anticancer activity against ovairan CSCs *in vivo* with no toxicity.

3.5. Bola/IM Achieves a High Tumor-Oriented Accumulation with Enhanced Drug Delivery Efficiency. To gain a better understanding of the promising antitumor activity exhibited by Bola/IM, we coencapsulated the near-infrared fluorescence probe DiR within the Bola/IM nanoparticles (referred to as Bola/IM/DiR hereafter) to track their

https://doi.org/10.1021/acsami.4c12857
ACS Appl. Mater. Interfaces XXXX, XXX, XXX−XXX

biodistribution *in vivo* in tumor-bearing xenograft mice. It should be mentioned here that we could not use DiR-labeled IM as a control in our biodistribution study since it would not be representative of IM, the structural properties of the small molecule IM being largely overshadowed by those of the much larger DiR when conjugated. Our results showed that Bola/IM/DiR exhibited a much stronger and more localized fluorescence signal in tumor compared to the PBS and naked DiR controls at 8 h, with peak fluorescence observed at 48 h post intravenous injection (Figure 4a,b). This indicates that the bola-dendrimer nanoformulation prolonged the retention of loaded cargos in the circulating system, thereby facilitating their tumor-oriented accumulation *via* the EPR effect. Importantly, the DiR-labeled Bola/IM also penetrated deeper within the tumor tissues and spread further around the blood vessels compared to free DiR, as indicated in Figure 4c. This finding is particularly important for targeting CSCs most deeply buried within the bulky tumor tissue.

We also used confocal microscopy to further examine the penetration of the DiR-encapsulated Bola/IM (Bola/IM/DiR) within tumor spheroids under nonadherent conditions, which most closely mimics malignant ascites in advanced/metastatic stages of ovarian carcinoma. Fluorescence imaging revealed significantly stronger and deeper penetration of Bola/IM/DiR within the spheroids compared to the controls of PBS and DiR alone (Figure 4d). These findings were consistent with our *in vivo* studies (Figure 4c) and further demonstrate the ability of Bola/IM to penetrate deep within tumors, where deep-seated CSCs can be effectively targeted.

Previously we have demonstrated that Bola-dendrimers possess favorable properties in response to ROS-rich conditions.[26,27] Cancer cells have been shown to have higher levels of ROS compared to normal tissue.[36,37] ROS signaling, by driving the epithelial-mesenchymal transition, can induce cells to acquire stem-like properties.[38] In our study, we observed higher levels of ROS in HEYA8 CSCs compared to those in non-CSCs (Figure 4e). Interestingly, the fluorescent-labeled Bola/IM (Bola/IM/DiR) concomitantly colocalized with regions of high ROS expression in CSCs and its levels decreased upon inhibition of ROS with NAC (Figures 4f and S6). These findings confirm the higher uptake of Bola/IM in CSCs with high ROS levels and may also partly explain the effectiveness of Bola/IM against CSCs and not non-CSCs. Indeed, Bola/IM may be able to selectively target and eradicate CSCs in ovarian cancer by exploiting the elevated ROS levels in these cells.

Further investigation into the *in vivo* kinetic behavior of Bola/IM revealed that Bola/IM had a 2.8-fold higher absorption (IM AUC_{last} = 1180, Bola/IM AUC_{last}= 3260) and 50% lower elimination rate (IM $K_{el/h}$ = 0.654, Bola/IM $K_{el/h}$ = 0.356) compared to naked IM, suggesting a higher bioavailability and longer circulation retention of Bola/IM. Importantly, Bola/IM reached the maximum concentration (T_{max}) in the blood in a shorter amount of time and took longer to be reduced by half ($T_{1/2}$) compared to naked IM, confirming the prolonged duration of Bola/IM in the body (Figure 4g). In addition, the mean residence time (MRT) of Bola/IM was 1.4-fold longer (Figure 4g), with a higher mean concentration at 24 h compared with naked IM (Figure 4h), indicating that less frequent treatment with Bola/IM at lower doses could lead to the desired therapeutic effects. These results demonstrate the promising tumor-targeting ability of Bola/IM with enhanced drug delivery efficiency, further highlighting its potential as a promising therapeutic strategy for ovarian cancer.

3.6. Chemosensitizing Effects of the Bola/IM Nanoformulation *In Vivo*. We previously found that c-Kit inhibition could reduce the chemoresistance of ovarian CSCs. In this study, we established a patient-derived xenograft mouse model to examine whether Bola/IM could sensitize ovarian cancer to chemotherapies (Figure 5a). We found that the combination of the first-line chemotherapeutic agent for ovarian cancer, cisplatin, with Bola/IM produced synergistic actions to suppress metastatic tumor growth (Figure 5b). We obtained similar findings using patient-derived organoids (Figure 5c). Immunochemical analysis showed a decrease in expression levels of two downstream interaction partners of c-Kit, HRP2, and β-catenin, in tumor tissues upon Bola/IM treatment (Figure 5d), which were further reduced upon a combination of Bola/IM with cisplatin treatment (Figure 5d). Moreover, c-Kit expression is higher in patients who died of disease (DOD) compared with those alive with no evidence of disease (NED) (Figure S7). Collectively, these results confirm the effective anticancer activity of Bola/IM and the synergistic effect of combining it with cisplatin in treating ovarian cancer.

To further evaluate the potential toxicity of Bola/IM and its combination with cisplatin, we conducted histopathological analyses of major organs and blood biochemistry analyses in treated mice. Hematoxylin and eosin staining of the heart, liver, spleen, lungs, and kidneys showed no histological alterations (Figure 5e). Blood biochemical analysis revealed that neither Bola/IM nor its combination with cisplatin caused any significant increase in ALP, AST, or creatine kinase (Figure 5f), indicating the absence of damage to liver and kidney functions or any adverse effects on normal tissues. In addition, we observed no significant weight loss in the mice during the treatment (Figure S8a) and no apparent changes in the livers upon sacrifice (Figure S8b), suggesting that the doses administered were well-tolerated by the mice. Altogether, these data confirm the safety and potential efficacy of Bola/IM as a nanoformulation for the treatment of metastatic ovarian cancer, addressing an urgent, yet unmet, medical need.

4. DISCUSSION

Targeting CSCs, which are associated with drug resistance and recurrence in many tumors, has emerged as a promising treatment strategy for various cancers including metastatic ovarian cancer. However, targeting CSCs has proven to be challenging due to their rarity, quiescent nature, and deep location within bulky tumors. Considering that c-Kit has been identified as a functional marker and a potential target for CSCs, and that the clinical anticancer drug imatinib (IM) targets c-Kit, we developed a nanodrug system based on the bola-amphiphilic dendrimer Bola to effectively deliver IM for enhanced efficacy against CSCs, acting through a unique, tumor-specific β-catenin/HRP2 axis. We utilized cell lines, patient-derived ascites, organoid models, and metastatic ovarian cancer mouse models to evaluate the efficacy of this approach. In addition, combining Bola/IM with chemotherapeutic drugs shows synergistic anticancer activity without any adverse effects, highlighting its potential as a promising therapeutic strategy. Despite clinical trials of IM on patients with primary or recurrent ovarian cancer yielding unsatisfactory results, our nanodrug system holds promise for effectively targeting CSCs and improving IM treatment of ovarian cancer.

Dendrimers are nanosized molecules characterized by precise structures and cooperative multivalence. In this study, we demonstrated the effectiveness of a bola-amphiphilic dendrimer

https://doi.org/10.1021/acsami.4c12857
ACS Appl. Mater. Interfaces XXXX, XXX, XXX−XXX

for the delivery of IM. This delivery system offers several advantages: (i) high drug-loading capacity, allowing for effective therapeutic potency; (ii) small size (ca. 30 nm), enabling passive tumor targeting and deep tumor penetration to reach the deep-seated CSCs; (iii) higher uptake in CSCs with high levels of ROS, potentially enhancing the selective targeting of CSCs; (iv) overcomes drug efflux and drug resistance; (v) inhibits the β-catenin/HRP2 signaling pathway, which is implicated in CSC maintenance; and (vi) effective anticancer activity, both as a standalone treatment or in combination with the clinical drugs paclitaxel and cisplatin. These findings highlight the successful implication of dendrimer nanotechnology in combating CSCs to overcome drug resistance and enhance the potency of anticancer drugs.

Nanotechnology-based drug delivery offers the advantage of specifically targeting tumor tissue through passive targeting *via* the EPR effect, which results from leaky vasculature and dysfunctional lymphatic drainage in the tumor microenvironment. Furthermore, many cancer cells exhibit activated macropinocytosis, promoting endocytosis-mediated uptake of nanoparticles while bypassing drug efflux mechanisms. As a result, nanotechnology-based therapeutics often demonstrate improved therapeutic efficacy with reduced adverse effects. Previous studies have reported various nanoformulations of IM using poly(lactide-*co*-glycolide) or gold nanoparticles to increase its efficacy and reduce its cytotoxicity.[39,40] However, none of these studies have described an optimal delivery system that effectively targets tumor tissue and exhibits a favorable biodistribution and pharmacokinetic profile. Such a delivery system is crucial for enabling the effective anticancer activity of IM against metastatic ovarian cancer while minimizing its side effects. In this study, we have demonstrated for the first time that Bola/IM rapidly accumulated at the tumor sites *via* the EPR effect and penetrated deep within the tumor. The encapsulation of IM by Bola led to the nanodrug (Bola/IM) formulation with a size of 30 nm, facilitating the cellular uptake *via* endocytosis and enhancing intracellular IM concentration while bypassing efflux mechanisms at the plasma membrane. Moreover, Bola/IM effectively promoted uptake into ROS-rich cancer cells and inhibited drug efflux pumps. Importantly, while Bola/IM enhanced the antitumor activity of IM, it did not cause noticeable side effects or prominent toxicity. These findings align with our previous studies, where encapsulation of anticancer drugs such as paclitaxel, doxorubicin, and rapamycin within amphiphilic dendrimers significantly reduces off-target toxicity.[23−25] In addition, the higher AUC and slower drug clearance rate observed in our study are attributed to faster accumulation at the tumor site and longer retention of Bola/IM in the circulation. This suggests that lower and less frequent dosing of IM may suffice when encapsulated within Bola, thereby reducing its potential toxicity.

Our proteomic profiling study revealed HRP2 as a novel target of β-catenin that is inhibited by Bola/IM, which is a significant finding. We demonstrated for the first time the essential role of HRP2 and its interaction with β-catenin in the expansion of CSCs and the development of drug resistance. HRP2 is frequently overexpressed in human hepatocellular carcinomas.[41] As a transcriptional activator, HRP2 contains crucial domains in its N-terminal region, which are involved in the recognition of active chromatin, regulation of the transcriptional and prosurvival activity, and interactions with other proteins. HRP2 is also overexpressed in various other human cancers[42−44] and serves as an unfavorable prognostic marker in intrahepatic cholangiocarcinoma[45] and gliomas.[46] Interestingly, blocking HRP2 has been shown to enhance the antitumor activities of targeted drugs and chemotherapy, suggesting that targeting HRP2 may overcome drug resistance.[47−49] Accordingly in ovarian cancer, high HRP2 expression is associated with poor clinical outcomes. In CSCs, the interaction between HRP2 and β-catenin is crucial for self-renewal and tumorigenesis. Our analysis demonstrated that IM inhibited their expression and interaction at much higher doses when used alone compared with when encapsulated within the Bola/IM nanoformulation. The relatively low expression of HRP2/β-catenin in normal tissues further supports the potential of targeting HRP2 as a safe and promising approach to treating metastatic ovarian cancer.

5. CONCLUSIONS

In this study, we demonstrate that the nanoformulation Bola/IM can empower the clinical anticancer drug IM in treating metastatic ovarian cancer by targeting cancer stem cells *via* the β-catenin-HRP2 signaling axis. Previous clinical trials of IM as monotherapy or combination therapy have yielded unsatisfactory results for treating patients with primary or recurrent ovarian cancer.[50−52] Despite the initial response of most (75%) ovarian cancer patients to chemotherapy, nearly all eventually relapse due to the development of drug resistance, resulting in poor response or failure of chemotherapy. The high expression of drug transporters, such as P-glycoprotein and ABCG2, is a major cause of drug resistance in ovarian cancer. We demonstrate in this study that the nanoformulation Bola/IM resulting from the encapsulation of IM by a bola-amphiphilic dendrimer Bola can decrease the expression of P-glycoprotein and ABCG2, leading to a coordinated decrease in drug efflux and an increase in apoptosis. Furthermore, when administered in combination with the clinical drugs cisplatin and paclitaxel, Bola/IM acts to sensitize CSCs to these chemotherapeutic drugs.[7] Our finding of a synergistic effect when combining Bola/IM and cisplatin in metastatic ovarian cancer suggests that other combination treatments with nanodrug formulations warrant further investigation. Such a strategy is expected to enhance the therapeutic effectiveness of targeted or immunotherapeutic drugs while reducing the morbidity associated with conventional cytotoxic chemotherapy. The small number of patients available for analysis and the use of immunodeficient mice may limit the applicability of the findings. Further research along these lines will enhance the robustness of the study and its clinical applications.

■ ASSOCIATED CONTENT

Data Availability Statement

All the data related to this study are presented in the manuscript and Supporting Information.

Supporting Information

The Supporting Information is available free of charge at https://pubs.acs.org/doi/10.1021/acsami.4c12857.

Nanoformulation of imatinib using the bola-amphiphilic dendrimer; no body weights loss was caused upon Bola/IM treatments; and proteomic data (PDF)

■ AUTHOR INFORMATION

Corresponding Authors

Xiaoxuan Liu − *State Key Laboratory of Natural Medicines, Jiangsu Key Laboratory of Drug Discovery for Metabolic Diseases, Center of Advanced Pharmaceuticals and*

https://doi.org/10.1021/acsami.4c12857
ACS Appl. Mater. Interfaces XXXX, XXX, XXX−XXX

Biomaterials, China Pharmaceutical University, Nanjing 211198, China; Email: xiaoxuanliu@cpu.edu.cn

Ling Peng − *Aix-Marseille Université, CNRS, Centre Interdisciplinaire de Nanoscience de Marseille, Equipe Labellisée Ligue Contre le Cancer, 13288 Marseille, France*; orcid.org/0000-0003-3990-5248; Email: ling.peng@univ-amu.fr

Alice S. T. Wong − *School of Biological Sciences, University of Hong Kong, Pokfulam, Hong Kong 999077, China*; orcid.org/0000-0002-0676-6475; Email: awong1@hku.hk

Authors

Zeyu Shi − *School of Biological Sciences, University of Hong Kong, Pokfulam, Hong Kong 999077, China; Laboratory for Synthetic Chemistry and Chemical Biology Limited, Pokfulam, Hong Kong 999077, China;* Present Address: Department of Anesthesia and Intensive Care, Prince of Wales Hospital, The Chinese University of Hong Kong, Hong Kong, China

Margarita Artemenko − *School of Biological Sciences, University of Hong Kong, Pokfulam, Hong Kong 999077, China*

Weiyu Yu − *School of Biological Sciences, University of Hong Kong, Pokfulam, Hong Kong 999077, China*

Ming Zhang − *School of Biological Sciences, University of Hong Kong, Pokfulam, Hong Kong 999077, China*

Canhui Yi − *School of Biological Sciences, University of Hong Kong, Pokfulam, Hong Kong 999077, China*

Peng Chen − *State Key Laboratory of Natural Medicines, Jiangsu Key Laboratory of Drug Discovery for Metabolic Diseases, Center of Advanced Pharmaceuticals and Biomaterials, China Pharmaceutical University, Nanjing 211198, China*

Shuting Lin − *State Key Laboratory of Natural Medicines, Jiangsu Key Laboratory of Drug Discovery for Metabolic Diseases, Center of Advanced Pharmaceuticals and Biomaterials, China Pharmaceutical University, Nanjing 211198, China*

Zhancun Bian − *State Key Laboratory of Natural Medicines, Jiangsu Key Laboratory of Drug Discovery for Metabolic Diseases, Center of Advanced Pharmaceuticals and Biomaterials, China Pharmaceutical University, Nanjing 211198, China; Aix-Marseille Université, CNRS, Centre Interdisciplinaire de Nanoscience de Marseille, Equipe Labellisée Ligue Contre le Cancer, 13288 Marseille, France*

Baoping Lian − *State Key Laboratory of Natural Medicines, Jiangsu Key Laboratory of Drug Discovery for Metabolic Diseases, Center of Advanced Pharmaceuticals and Biomaterials, China Pharmaceutical University, Nanjing 211198, China*

Fanzhen Meng − *State Key Laboratory of Natural Medicines, Jiangsu Key Laboratory of Drug Discovery for Metabolic Diseases, Center of Advanced Pharmaceuticals and Biomaterials, China Pharmaceutical University, Nanjing 211198, China*

Jiaxuan Chen − *State Key Laboratory of Natural Medicines, Jiangsu Key Laboratory of Drug Discovery for Metabolic Diseases, Center of Advanced Pharmaceuticals and Biomaterials, China Pharmaceutical University, Nanjing 211198, China; Aix-Marseille Université, CNRS, Centre Interdisciplinaire de Nanoscience de Marseille, Equipe Labellisée Ligue Contre le Cancer, 13288 Marseille, France*; orcid.org/0000-0002-8103-2009

Tom Roussel − *Aix-Marseille Université, CNRS, Centre Interdisciplinaire de Nanoscience de Marseille, Equipe Labellisée Ligue Contre le Cancer, 13288 Marseille, France*

Ying Li − *State Key Laboratory of Natural Medicines, Jiangsu Key Laboratory of Drug Discovery for Metabolic Diseases, Center of Advanced Pharmaceuticals and Biomaterials, China Pharmaceutical University, Nanjing 211198, China*

Karen K. L. Chan − *Department of Obstetrics and Gynecology, Queen Mary Hospital, University of Hong Kong, Pokfulam, Hong Kong 999077, China*

Philip P. C. Ip − *Department of Pathology, Queen Mary Hospital, University of Hong Kong, Pokfulam, Hong Kong 999077, China*

Hung-Cheng Lai − *Department of Obstetrics and Gynecology, School of Medicine, College of Medicine, Taipei Medical University, Taipei 11031, Taiwan; Department of Obstetrics and Gynecology, Shuang Ho Hospital, Taipei Medical University, Taipei 23561, Taiwan*

Sally K. Y. To − *School of Biological Sciences, University of Hong Kong, Pokfulam, Hong Kong 999077, China; Laboratory for Synthetic Chemistry and Chemical Biology Limited, Pokfulam, Hong Kong 999077, China*

Complete contact information is available at: https://pubs.acs.org/10.1021/acsami.4c12857

Author Contributions

◆Z.S. and M.A. contributed equally to this work. Z.S., M.A., W.Y., and M.Z. performed cellular experiments. Z.S., M.A., M.Z., and S.L. performed animal experiments. Z.S., M.A., and S.T. contributed to conceptualization and methodology. Z.S. wrote the original draft. Z.S., S.T., X.L., P.L., and A.W. reviewed and edited the manuscript. Z.B., B.L., F.M., J.C., T.R., and Y.L. performed nanoparticle synthesis and drug encapsulation. K.C., P.I., and H.C. provided clinical samples. X.L., L.P., and A.W. supervised the project.

Notes

The authors declare no competing financial interest.

■ ACKNOWLEDGMENTS

This study received support from the Health and Medical Research Fund 06173496 (A.S.T.W.) and the "Laboratory for Synthetic Chemistry and Chemical Biology" through the Health@InnoHK Program initiated by the Innovation and Technology Commission, HKSAR.

■ REFERENCES

(1) Huang, J.; Chan, W. C.; Ngai, C. H.; Lok, V.; Zhang, L.; Lucero-Prisno, D. E.; Xu, W.; Zheng, Z.-J.; Elcarte, E.; Withers, M.; Wong, M. C. S.; on behalf of NCD Global Health Research Group of Association of Pacific Rim Universities (APRU). Worldwide Burden, Risk Factors, and Temporal Trends of Ovarian Cancer: A Global Study. *Cancers* **2022**, *14* (9), No. 2230.

(2) Matulonis, U. A.; Sood, A. K.; Fallowfield, L.; Howitt, B. E.; Sehouli, J.; Karlan, B. Y. Ovarian Cancer. *Nat. Rev. Dis. Primer* **2016**, *2* (1), No. 16061.

(3) Lheureux, S.; Gourley, C.; Vergote, I.; Oza, A. M. Epithelial Ovarian Cancer. *Lancet* **2019**, *393* (10177), 1240−1253.

(4) McMullen, M.; Karakasis, K.; Rottapel, R.; Oza, A. M. Advances in Ovarian Cancer, from Biology to Treatment. *Nat. Cancer* **2021**, *2* (1), 6−8.

(5) Marchetti, C.; De Felice, F.; Romito, A.; Iacobelli, V.; Sassu, C. M.; Corrado, G.; Ricci, C.; Scambia, G.; Fagotti, A. Chemotherapy Resistance in Epithelial Ovarian Cancer: Mechanisms and Emerging Treatments. *Semin. Cancer Biol.* **2021**, *77*, 144−166.

(6) Lytle, N. K.; Barber, A. G.; Reya, T. Stem Cell Fate in Cancer Growth, Progression and Therapy Resistance. *Nat. Rev. Cancer* **2018**, *18* (11), 669−680.
(7) Chau, W. K.; Ip, C. K.; Mak, A. S. C.; Lai, H.-C.; Wong, A. S. T. C-Kit Mediates Chemoresistance and Tumor-Initiating Capacity of Ovarian Cancer Cells through Activation of Wnt/β-Catenin−ATP-Binding Cassette G2 Signaling. *Oncogene* **2013**, *32* (22), 2767−2781.
(8) Goeppert, B.; Frauenschuh, L.; Zucknick, M.; Stenzinger, A.; Andrulis, M.; Klauschen, F.; Joehrens, K.; Warth, A.; Renner, M.; Mehrabi, A.; Hafezi, M.; Thelen, A.; Schirmacher, P.; Weichert, W. Prognostic Impact of Tumour-Infiltrating Immune Cells on Biliary Tract Cancer. *Br. J. Cancer* **2013**, *109* (10), 2665−2674.
(9) Cohen, P.; Cross, D.; Jänne, P. A. Kinase Drug Discovery 20 Years After Imatinib: Progress and Future Directions. *Nat. Rev. Drug Discovery* **2021**, *20* (7), 551−569.
(10) Chopade, P.; Akard, L. P. Improving Outcomes in Chronic Myeloid Leukemia Over Time in the Era of Tyrosine Kinase Inhibitors. *Clin. Lymphoma, Myeloma Leuk.* **2018**, *18* (11), 710−723.
(11) Shi, J.; Kantoff, P. W.; Wooster, R.; Farokhzad, O. C. Cancer Nanomedicine: Progress, Challenges and Opportunities. *Nat. Rev. Cancer* **2017**, *17* (1), 20−37.
(12) Bhatia, S. N.; Chen, X.; Dobrovolskaia, M. A.; Lammers, T. Cancer Nanomedicine. *Nat. Rev. Cancer* **2022**, *22* (10), 550−556.
(13) Mitchell, M. J.; Billingsley, M. M.; Haley, R. M.; Wechsler, M. E.; Peppas, N. A.; Langer, R. Engineering Precision Nanoparticles for Drug Delivery. *Nat. Rev. Drug Discovery* **2021**, *20* (2), 101−124.
(14) Shi, Y.; Van Der Meel, R.; Chen, X.; Lammers, T. The EPR Effect and beyond: Strategies to Improve Tumor Targeting and Cancer Nanomedicine Treatment Efficacy. *Theranostics* **2020**, *10* (17), 7921−7924.
(15) Fang, J.; Islam, W.; Maeda, H. Exploiting the Dynamics of the EPR Effect and Strategies to Improve the Therapeutic Effects of Nanomedicines by Using EPR Effect Enhancers. *Adv. Drug Delivery Rev.* **2020**, *157*, 142−160.
(16) Li, X.; Hu, Y.; Zhang, X.; Shi, X.; Parak, W. J.; Pich, A. Transvascular Transport of Nanocarriers for Tumor Delivery. *Nat. Commun.* **2024**, *15*, No. 8172.
(17) Nel, A.; Ruoslahti, E.; Meng, H. New Insights into "Permeability" as in the Enhanced Permeability and Retention Effect of Cancer Nanotherapeutics. *ACS Nano* **2017**, *11*, 9567−9569.
(18) Lyu, Z.; Peng, L. Potent Drugless Dendrimers. *Nat. Biomed. Eng.* **2017**, *1* (9), 686−688.
(19) Kannan, R. M.; Nance, E.; Kannan, S.; Tomalia, D. A. Emerging Concepts in Dendrimer-Based Nanomedicine: From Design Principles to Clinical Applications. *J. Int. Med.* **2014**, *276* (6), 579−617.
(20) Lyu, Z.; Ding, L.; Tintaru, A.; Peng, L. Self-Assembling Supramolecular Dendrimers for Biomedical Applications: Lessons Learned from Poly (Amidoamine) Dendrimers. *Acc. Chem. Res.* **2020**, *53* (12), 2936−2949.
(21) Chen, J.; Zhu, D.; Liu, X.; Peng, L. Amphiphilic Dendrimer Vectors for RNA Delivery: State-of-the-Art and Future Perspective. *Acc. Mater. Res.* **2022**, *3* (5), 484−497.
(22) Percec, V.; Wilson, D. A.; Leowanawat, P.; Wilson, C. J.; Hughes, A. D.; Kaucher, M. S.; Hammer, D. A.; Levine, D. H.; Kim, A. J.; Bates, F. S.; Davis, K. P.; Lodge, T. P.; Klein, M. L.; DeVane, R. H.; Aqad, E.; Rosen, B. M.; Argintaru, A. O.; Sienkowska, M. J.; Rissanen, K.; Nummelin, S.; Ropponen, J. Self-Assembly of Janus Dendrimers into Uniform Dendrimersomes and Other Complex Architectures. *Science* **2010**, *328* (5981), 1009−1014.
(23) Jiang, Y.; Lyu, Z.; Ralahy, B.; Liu, J.; Roussel, T.; Ding, L.; Tang, J.; Kosta, A.; Giorgio, S.; Tomasini, R.; Liang, X.-J.; Dusetti, N.; Iovanna, J.; Peng, L. Dendrimer Nanosystems for Adaptive Tumor-Assisted Drug Delivery *via* Extracellular Vesicle Hijacking. *Proc. Natl. Acad. Sci. U.S.A.* **2023**, *120* (7), No. e2215308120.
(24) Wei, T.; Chen, C.; Liu, J.; Liu, C.; Posocco, P.; Liu, X.; Cheng, Q.; Huo, S.; Liang, Z.; Fermeglia, M.; Pricl, S.; Liang, X.-J.; Rocchi, P.; Peng, L. Anticancer Drug Nanomicelles Formed by Self-Assembling Amphiphilic Dendrimer to Combat Cancer Drug Resistance. *Proc. Natl. Acad. Sci. U.S.A.* **2015**, *112* (10), 2978−2983.
(25) Liu, J.; Chen, C.; Wei, T.; Gayet, O.; Loncle, C.; Borge, L.; Dusetti, N.; Ma, X.; Marson, D.; Laurini, E.; Pricl, S.; Gu, Z.; Iovanna, J.; Peng, L.; Liang, X. Dendrimeric Nanosystem Consistently Circumvents Heterogeneous Drug Response and Resistance in Pancreatic Cancer. *Exploration* **2021**, *1* (1), 21−34.
(26) Chen, J.; Zhu, D.; Lian, B.; Shi, K.; Chen, P.; Li, Y.; Lin, W.; Ding, L.; Long, Q.; Wang, Y.; Laurini, E.; Lan, W.; Li, Y.; Tintaru, A.; Ju, C.; Zhang, C.; Pricl, S.; Iovanna, J.; Liu, X.; Peng, L. Cargo-Selective and Adaptive Delivery of Nucleic Acid Therapeutics by Bola-Amphiphilic Dendrimers. *Proc. Natl. Acad. Sci. U.S.A.* **2023**, *120* (21), No. e2220787120.
(27) Liu, X.; Wang, Y.; Chen, C.; Tintaru, A.; Cao, Y.; Liu, J.; Ziarelli, F.; Tang, J.; Guo, H.; Rosas, R.; Giorgio, S.; Charles, L.; Rocchi, P.; Peng, L. A Fluorinated Bola-Amphiphilic Dendrimer for On-Demand Delivery of siRNA, *via* Specific Response to Reactive Oxygen Species. *Adv. Funct. Mater.* **2016**, *26*, 8594−8603.
(28) Bhattacharya, A. Self-Assembly and Biophysical Properties of Archaeal Lipids. *Emerg. Top. Life Sci.* **2022**, *6* (6), 571−582.
(29) Chen, H.; Viel, S.; Ziarelli, F.; Peng, L. 19F NMR: A Valuable Tool for Studying Biological Events. *Chem. Soc. Rev.* **2013**, *42* (20), 7971−7982.
(30) Lyu, Z.; Ralahy, B.; Perles-Barbacaru, T. A.; Ding, L.; Jiang, Y.; Lian, B.; Roussel, T.; Liu, X.; Galanakou, C.; Laurini, E.; Tintaru, A.; Giorgio, S.; Pricl, S.; Liu, X.; Iovanna, J.; Bernard, M.; Viola, A.; Peng, L. Self-Assembling Dendrimer Nanosystems for Specific Fluorine Magnetic Resonance Imaging and Effective Theranostic Treatment of Tumors. *Proc. Natl. Acad. Sci. U.S.A.* **2024**, *121*, No. e2322403121.
(31) Dean, M.; Fojo, T.; Bates, S. Tumour Stem Cells and Drug Resistance. *Nat. Rev. Cancer* **2005**, *5*, 275−284.
(32) Ughachukwu, P.; Unekwe, P. Efflux Pump-Mediated Resistance in Chemotherapy. *Ann. Med. Health Sci. Res.* **2012**, *2*, 191−198.
(33) Su, Z.; Dong, S.; Zhao, S. C.; Liu, K.; Tan, Y.; Jiang, X.; Assaraf, Y. G.; Qin, B.; Chen, Z. S.; Zou, C. Novel Nanomedicines to Overcome Cancer Multidrug Resistance. *Drug Resistance Updates* **2021**, *58*, No. 100777.
(34) Jayashankar, V.; Edinger, A. L. Macropinocytosis Confers Resistance to Therapies Targeting Cancer Anabolism. *Nat. Commun.* **2020**, *11* (1), No. 1121.
(35) Song, S.; Zhang, Y.; Ding, T.; Ji, N.; Zhao, H. The Dual Role of Macropinocytosis in Cancers: Promoting Growth and Inducing Methuosis to Participate in Anticancer Therapies as Targets. *Front. Oncol.* **2021**, *10*, No. 570108.
(36) Nakamura, H.; Takada, K. Reactive Oxygen Species in Cancer: Current Findings and Future Directions. *Cancer Sci.* **2021**, *112* (10), 3945−3952.
(37) Liao, Z.; Chua, D.; Tan, N. S. Reactive Oxygen Species: A Volatile Driver of Field Cancerization and Metastasis. *Mol. Cancer* **2019**, *18* (1), No. 65.
(38) Cheung, E. C.; Vousden, K. H. The Role of ROS in Tumour Development and Progression. *Nat. Rev. Cancer* **2022**, *22* (5), 280−297.
(39) Sadat Shandiz, S. A.; Shafiee Ardestani, M.; Shahbazzadeh, D.; Assadi, A.; Ahangari Cohan, R.; Asgary, V.; Salehi, S. Novel Imatinib-Loaded Silver Nanoparticles for Enhanced Apoptosis of Human Breast Cancer MCF-7 Cells. *Artif. Cells, Nanomed., Biotechnol.* **2017**, *45* (6), 1082−1091.
(40) Sheeba, C. J.; Marslin, G.; Revina, A. M.; Khandelwal, V.; Balakumar, K.; Prakash, J.; Franklin, G. Delivery as Nanoparticles Reduces Imatinib Mesylate-Induced Cardiotoxicity and Improves Anticancer Activity. *Int. J. Nanomed.* **2015**, 3163−3170.
(41) Gao, K.; Xu, C.; Jin, X.; Wumaier, R.; Ma, J.; Peng, J.; Wang, Y.; Tang, Y.; Yu, L.; Zhang, P. HDGF-Related Protein-2 (HRP-2) Acts as an Oncogene to Promote Cell Growth in Hepatocellular Carcinoma. *Biochem. Biophys. Res. Commun.* **2015**, *458* (4), 849−855.
(42) Wei, Y.; Fu, J.; Zhang, H.; Ling, Y.; Tang, X.; Liu, S.; Yu, M.; Liu, F.; Zhuang, G.; Qian, H.; Zhang, K.; Yang, P.; Yang, X.; Yang, Q.; Ge, S.; Zhang, B.; Tan, Y.; Li, L.; Wang, H. N6-Methyladenosine Modification Promotes Hepatocarcinogenesis through Circ-CDYL-Enriched and

https://doi.org/10.1021/acsami.4c12857
ACS Appl. Mater. Interfaces XXXX, XXX, XXX−XXX

EpCAM-Positive Liver Tumor-Initiating Exosomes. *iScience* **2023**, *26* (10), No. 108022.
(43) Zhang, X.; Zheng, W.; Jiang, W.; Lin, R.; Xing, C. Long Non-Coding RNA SNHG3 Accelerates Progression in Glioma by Modulating miR-384/HDGF Axis. *Open Life Sci.* **2020**, *15* (1), 654−664.
(44) Wang, Q.; Chen, C.; Ding, Q.; Zhao, Y.; Wang, Z.; Chen, J.; Jiang, Z.; Zhang, Y.; Xu, G.; Zhang, J.; Zhou, J.; Sun, B.; Zou, X.; Wang, S. METTL3-Mediated m ^{6} A Modification of HDGF mRNA Promotes Gastric Cancer Progression and Has Prognostic Significance. *Gut* **2020**, *69* (7), 1193−1205.
(45) Guo, S.; Liu, H.; Liu, Y.-F.; Liu, L.; Sun, Q.; Cui, X.-J. Hepatoma-Derived Growth Factor: A Novel Prognostic Biomarker in Intrahepatic Cholangiocarcinoma. *Tumour Biol.* **2015**, *36* (1), 353−364.
(46) Yang, Y.; Liang, S.; Li, Y.; Gao, F.; Zheng, L.; Tian, S.; Yang, P.; Li, L. Hepatoma-derived Growth Factor Functions as an Unfavorable Prognostic Marker of Human Gliomas. *Oncol. Lett.* **2017**, *14* (6), 7179−7184.
(47) Xiao, Q.; Qu, K.; Wang, C.; Kong, Y.; Liu, C.; Jiang, D.; Saiyin, H.; Jia, F.; Ni, C.; Chen, T.; Zhang, Y.; Zhang, P.; Qin, W.; Sun, Q.; Wang, H.; Yi, Q.; Liu, J.; Huang, H.; Yu, L. HDGF-Related Protein-3 Is Required for Anchorage-Independent Survival and Chemoresistance in Hepatocellular Carcinomas. *Gut* **2013**, *62* (3), 440−451.
(48) Zhao, J.; Ma, M. Z.; Ren, H.; Liu, Z.; Edelman, M. J.; Pan, H.; Mao, L. Anti-HDGF Targets Cancer and Cancer Stromal Stem Cells Resistant to Chemotherapy. *Clin. Cancer Res.* **2013**, *19* (13), 3567−3576.
(49) Han, S.; Tian, Z.; Tian, H.; Han, H.; Zhao, J.; Jiao, Y.; Wang, C.; Hao, H.; Wang, S.; Fu, J.; Xue, D.; Sun, H.; Li, P. HDGF Promotes Gefitinib Resistance by Activating the PI3K/AKT and MEK/ERK Signaling Pathways in Non-Small Cell Lung Cancer. *Cell Death Discovery* **2023**, *9*, No. 181.
(50) M.D. Anderson Cancer Center. *A Phase II Study of Gleevec in Patients With Recurrent Platinum-Resistant, Taxane-Resistant Epithelial Ovarian Cancer, Primary Peritoneal Cancer, or Fallopian Tube Cancer*; Clinical trial registration NCT00510653, 2013. https://clinicaltrials.gov/study/NCT00510653.(accessed July 13, 2023).
(51) Matei, D. *Imatinib Mesylate (Gleevec, STI571) in Combination With Docetaxel (Taxotere) for the Treatment of Advanced, Platinum-Refractory Ovarian Cancer and Primary Peritoneal Carcinomatosis: Hoosier Oncology Group GYN03−62*; Clinical trial registration NCT00216112, 2016. https://clinicaltrials.gov/study/NCT00216112. (accessed July 13, 2023).
(52) NYU Langone Health. *Phase II Study of Paclitaxel With Imatinib Mesylate (Gleevec) in Taxane-Pretreated Ovarian and Other Cancers of Mullerian Origin*; Clinical trial registration NCT00840450, 2012. https://clinicaltrials.gov/study/NCT00840450. (accessed July 13, 2023).

https://doi.org/10.1021/acsami.4c12857
ACS Appl. Mater. Interfaces XXXX, XXX, XXX−XXX